**PAPER**

# Ion–ion and ion–solvent interactions in lithium imidazolide electrolytes studied by Raman spectroscopy and DFT models†

Johan Scheers,*[a] Leszek Niedzicki,[bc] Grażyna Z. Żukowska,[bc] Patrik Johansson,[ac] Władysław Wieczorek[bc] and Per Jacobsson[a]

Molecular level interactions are of crucial importance for the transport properties and overall performance of ion conducting electrolytes. In this work we explore ion–ion and ion–solvent interactions in liquid and solid polymer electrolytes of lithium 4,5-dicyano-(2-trifluoromethyl)-imidazolide (LiTDI)—a promising salt for lithium battery applications—using Raman spectroscopy and density functional theory calculations. High concentrations of ion associates are found in LiTDI:acetonitrile electrolytes, the vibrational signatures of which are transferable to PEO-based LiTDI electrolytes. The origins of the spectroscopic changes are interpreted by comparing experimental spectra with simulated Raman spectra of model structures. Simple ion pair models in vacuum identify the imidazole nitrogen atom of the TDI anion to be the most important coordination site for Li$^+$, however, including implicit or explicit solvent effects lead to qualitative changes in the coordination geometry and improved correlation of experimental and simulated Raman spectra. To model larger aggregates, solvent effects are found to be crucial, and we finally suggest possible triplet and dimer ionic structures in the investigated electrolytes. In addition, the effects of introducing water into the electrolytes—*via* a hydrate form of LiTDI—are discussed.

## 1. Introduction

One of the main challenges for expanding the lithium battery market outside the scope of consumer electronics is battery safety. A key component in this respect is the electrolyte and vast research efforts on lithium battery electrolytes are currently aimed at finding new salt and solvent combinations to replace the archetypic LiPF$_6$ + organic carbonate electrolytes; the safety limitations of which are well documented.[1–3] Focus is on thermally, chemically, and electrochemically stable alternatives to improve the overall safety of the battery, while limiting the use of costly additives. High performance electrolytes require high lithium ion conductivity at all working temperatures, a property dependent on—amongst other factors—the ease of lithium salt dissolution, the strength of anion–cation and ion–solvent interactions, and anion size.

Of the suggested alternatives to LiPF$_6$, the lithium fluoroalkyl imidazole and benzimidazole salts represent interesting alternatives,[4–7] with mixed features of more recent lithium salts (*e.g.* LiPF$_3$(C$_2$F$_5$)$_3$ (LiFAP)[8,9] and the triazolate LiC$_4$N$_5$ (LiTADC);[10,11] they incorporate both fluoroalkyl (–C$_x$F$_{2x+1}$) and cyano (–CN) groups as stable electronegative substituents on an imidazole core. The smallest member of this family of salts is lithium 4,5-dicyano-(2-trifluoromethyl)imidazolide (LiTDI).‡[12]

Performance tests of LiTDI, and its larger (2-pentafluoroethyl) relative LiPDI, have shown that these salts are thermally and electrochemically robust, do not corrode aluminium, and that PEGDME-based electrolytes thereof are stable in contact with the lithium metal.[4,5] Full battery tests of Li/EC:DMC/LiMn$_2$O$_4$ coin cells, with LiTDI or LiPDI, have shown overall cell performance on the same level as with LiPF$_6$.[13] The main advantages of the imidazole salts over LiPF$_6$ are their chemical stability and ease of handling. Unlike LiPF$_6$, which decomposes rapidly in the presence of water, LiTDI and LiPDI are stable

[a] *Department of Applied Physics, Chalmers University of Technology, SE-412 96 Göteborg, Sweden. E-mail: johan.scheers@chalmers.se; Fax: +46 31 772 2090; Tel: +46 31 772 3177*
[b] *Polymer Ionics Research Group, Faculty of Chemistry, Warsaw University of Technology, Noakowskiego 3, PL-00664 Warsaw, Poland*
[c] *ALISTORE-European Research Institute, France*

‡ List of abbreviations: ACN, acetonitrile; ACT, acetone; AN, acceptor number; C-PCM, conductor-like polarizable continuum model; DFT, density functional theory; DMC, dimethyl carbonate; DMSO, dimethyl sulfoxide; DN, donor number; EC, ethylene carbonate; G03 (G09), Gaussian 03 (09); PC, propylene carbonate; PCM, polarizable continuum model; PEGDME, poly(ethylene glycol) dimethyl ether; PEO, poly(ethylene oxide); TDI, 4,5-dicyano-(2-trifluoromethyl)-imidazolide; TGL, tri(ethylene glycol) dimethyl ether; SPE, solid polymer electrolyte; UAKS, united atom topological model; UFF, universal force field; vdW, van der Waals.

11136 | *Phys. Chem. Chem. Phys.*, 2011, **13**, 11136–11147

This journal is © the Owner Societies 2011

against water and have been applied to electrolytes in both hydrated and anhydrous forms, with no observable changes in electrochemical properties, not even when the electrolyte is in contact with a lithium metal surface.[13] This has been ascribed to the ability of the salt to act as a "moisture trap".

On the molecular level, ion association has been reported for LiTDI and LiPDI in propylene carbonate[7] and electrolytes based on oligoethers.[4] However, the estimated amount and type of associates in these electrolytes depend on the method used, since results of different techniques are interpreted in terms of different types of associates; solvent separated, solvent shared, or contact. Ion conductivity data, analyzed in the Fuoss–Krauss formalism, offer quantitative results on the total concentration of associates (contact + non-contact), which is found to be high in these electrolytes,[4] but provide no information on associate structures. Raman spectroscopy, on the other hand, provides indirect structural information, extractable from the shifts of individual vibrational bands—preferentially in combination with computed Raman spectra of different structural models. However, the absence of visible shifts in the explored systems indicates no or very few contact ion pairs, even at 1 M salt concentrations.[4,7] As a result, the specific interactions of these anions with the lithium cation and/or solvent molecules remain elusive.

Possible ion pair configurations have been suggested from density functional theory (DFT) calculations, but have so far not been unambiguously identified experimentally.[6] In contrast to earlier vibrational spectroscopic studies, which have focused on the $\nu$(CN) mode of the anions and on specific electrolyte systems,[4,7] we here take into account all Raman active modes of TDI and a range of organic electrolytes. Focus is on LiTDI:poly(ethylene oxide); a realistic solid polymer electrolyte (SPE) for battery application, and LiTDI:acetonitrile; a model system where significant spectroscopic changes can be observed. Differences in the spectroscopically observed number of bands and their positions are discussed in terms of solvent properties, ion–ion, and ion–solvent interactions, with attention given also to the role of water in the electrolytes, originating from the hydrated salts.

## 2. Experimental and computational methods

### 2.1 Electrolyte preparation

LiTDI was synthesized according to previously reported routines[5] and was therefore a hydrate of the approximate composition $LiTDI(H_2O)_{1/3}$.[13] The salt and the solvents: acetonitrile (ACN; Aldrich, anhydrous $\geq$ 99.8%, 0.786 g cm$^{-3}$), dimethyl sulfoxide (DMSO; Sigma, ACS reagent), 1,2-propylene carbonate (PC; Aldrich, anhydrous $\geq$ 99.7%), poly(ethylene glycol) dimethyl ether (PEGDME; Fluka, $M_w$ = 400 g mol$^{-1}$, 1.06 g cm$^{-3}$), and tri(ethylene glycol) dimethyl ether (TGL; Fluka, over molecular sieves, 0.986 g cm$^{-3}$), were handled in an argon dry box at all times ($<$1 ppm of H$_2$O). In addition three solvents: acetone (ACT; Merck, for analysis $\geq$ 99.8%), methanol (METH; Merck, for analysis $\geq$ 99.9%), and water (H$_2$O; Direct-Q Millipore; $\sigma$ = 0.056 $\mu$S cm$^{-1}$; 0.988 g cm$^{-3}$), were handled in normal atmosphere, in the preparation of the corresponding electrolytes. All solvents were used as

**Table 1** Properties of electrolyte solvents

| Solvent | Molecular formula | $\varepsilon$ | AN | DN |
|---|---|---|---|---|
| ACN | CH$_3$C≡N | 35.9 | 18.9 | 14.1 |
| ACT | (CH$_3$)$_2$C=O | 20.6 | 12.5 | 17.0 |
| DMSO | (CH$_3$)$_2$S=O | 46.5 | 19.3 | 29.8 |
| H$_2$O | H$_2$O | 78.4 | 54.8 | 18.0 |
| METH | CH$_3$OH | 32.7 | 41.3[17] | 19.0 |
| PC | C$_4$H$_6$O$_3$ | 64.9 | 18.3 | 15.1 |
| TGL | CH$_3$O–[CH$_2$CH$_2$O]$_3$–CH$_3$ | 7.6 | 10.5[16] | 14.0[16] |

$\varepsilon$ = Relative permittivitty;[14] AN = acceptor number;[15] DN = donor number.[15]

received. A summary of basic solvent properties: relative permittivities ($\varepsilon$)[14] and Gutmann acceptor/donor numbers (AN and DN),[15–17] is listed in Table 1.

Samples for the Raman measurements were prepared in volumes of 0.5–1 cm$^3$ and sealed in 4 cm$^3$ glass vials. For each solvent, LiTDI electrolytes were prepared with an initial salt concentration of 1.0 mol ($M_{LiTDI(H_2O)_{1/3}} \approx$ 198 g mol$^{-1}$) per dm$^{-3}$ of solvent. However, for convenience the concentrations are given as mol dm$^{-3}$ (M). More concentrated electrolytes were prepared for selected solvents; 4 M with water and TGL, and 2 M with ACN. Less concentrated samples, down to 0.05 M for ACN and PEGDME, were obtained by dilution.

SPEs were prepared from poly(ethylene oxide) (PEO; HO–[CH$_2$CH$_2$O]$_n$–H, PolySciences, $M_w$ = 5 × 10$^6$ g mol$^{-1}$, freeze dried for three days at 60 °C and 10$^{-2}$ mbar), ACN, and LiTDI. For these electrolytes, the lithium salt was pre-treated by drying under vacuum, at 80 °C for 72 h, after which the salt was considered to be anhydrous; ATR-spectra showed no water signatures (as opposed to the LiTDI hydrate) and qualitative changes in the TDI modes. Karl Fischer titration indicated a large reduction in water content from ~1700 ppm to $<$100 ppm after drying.

For the preparation of each unique SPE, 3 ml of a bulk solution of PEO in ACN (20 mg PEO per cm$^3$ ACN) was mixed with a 2 ml of LiTDI:ACN solution, to give 5 ml of LiTDI:PEO:ACN solutions with Li:O proportions equal to 1:8, 1:16, 1:21, 1:32, and 1:160. To ensure homogeneous solutions, the bulk PEO:ACN was stirred at room temperature for several days before use and the LiTDI:PEO:ACN mixtures were stirred for a day before transferring to Teflon dishes, 32 mm in diameter. The solvent was allowed to evaporate for several days over X13 molecular sieves in a closed poly-(propylene) box. The resulting SPEs, ~50 μm thick, were transferred to a Büchi oven, where the remaining solvent was evaporated under vacuum for 72 h, without heating. All preparation steps of the SPEs were made in the argon dry box.

To study the effect of water on LiTDI:ACN electrolytes, a 0.5 M electrolyte was used as the starting electrolyte for sequential addition of water. A water-free reference electrolyte of the same salt concentration was prepared from the anhydrous salt.

### 2.2 Spectroscopy

FT-Raman spectra were recorded on a Bruker IFS66 instrument equipped with a FRA 106 FT-Raman module and a Nd:YAG laser (1064 nm) as a laser source. The recording time for a

typical electrolyte spectrum was 2–5 h and 30 min for the solid salt. The laser power was 300 mW for the liquid samples and 100 mW for all solid samples.

### 2.3 Computations

All computations were performed within the Gaussian 03 (G03) or G09 software suites,[18] with the B3LYP/6-311+G(d) hybrid density functional[19,20] and Pople basis set.[21] The optimized anion structure and the computational approach for screening lithium ion pair structures have been reported elsewhere.[6] All vacuum calculations were performed in G03, while G09 was used for the implicit solvation calculations, because of the faster implementation and updated solvent parameters. The implicit model used was C-PCM;[22] the conductor-like screening model (COSMO)[23] in the framework of the polarizable continuum model (PCM),[24] with the default van der Waals (vdW) surface cavity and universal force field (UFF) radii. For the solvated anion and ion pairs, implicit calculations were repeated with either different radii; C-PCM in combination with united atom topological model (UAKS) radii, or a different model; PCM in combination with UFF. Differences were seen only in the case of different radii. Explicit solvated structures were obtained from the vacuum structures by adding up to three solvent molecules per Li^{+}. All structures were converged and were, in all but a few cases, confirmed as energy minima by computing the second derivatives of the energies with respect to nuclei displacements from the equilibrium structures. Structures which were not true energy minima had small imaginary modes due to difficulties of relaxing rotations of the –CH$_3$ or –CF$_3$ groups. As the rotational energies are negligible, all structures are considered minima.

For a reasonable comparison of Raman activities, $S_i$, calculated from partial third derivatives, with experimental intensities, $I_{i,exp}$, the former were transferred to intensity-like values $I_i$, according to eqn (1),[25] to take into account the variables of $I_{i,exp}$; the temperature, the laser wavenumber, $\nu_L$, and the Raman shift of normal mode i, $\nu_i$. The value of the constant, $C$, connected to the instrument response, was chosen to give a maximum intensity equal to one for the transferred Raman activities of TDI (in vacuum).

$$I_i = \frac{C[(\nu_L - \nu_i)^4]}{\nu_i\left(1 - \exp\left[-\left(\frac{hc\nu_i}{kT}\right)\right]\right)} S_i \qquad (1)$$

## 3. Results and discussion

In the following, promising vibrational bands for analyzing ion–ion and ion–solvent interactions of TDI are extracted from Raman spectra of several liquid LiTDI electrolytes. These bands are used to explore interactions of TDI with Li^{+}, solvents, and water, in electrolytes based on ACN, oligo- and polyethers. From a comparison of the experimental spectra with simulated Raman spectra of model structures, several possible ion-pair structures and larger ion associates are suggested.

### 3.1 Experimental Raman spectra of LiTDI electrolytes

**General features.** The TDI anion (Fig. 1) is a thirteen atom molecule with $C_s$ symmetry. In Fig. 2, the Raman spectra of
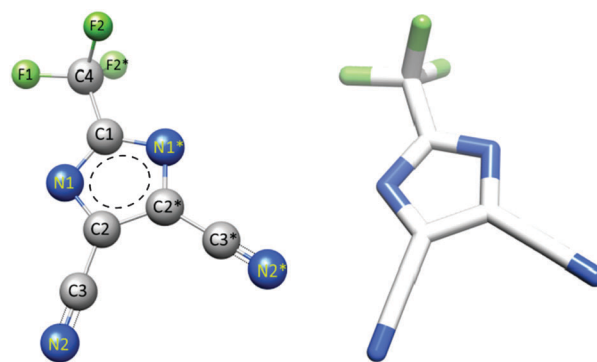


**Fig. 1** Schematic representations of the 4,5-dicyano-(2-trifluoro-methyl)imidazolide (TDI) anion. The atom numbering in the left structure is used in the mode assignment of the Raman spectrum of TDI.
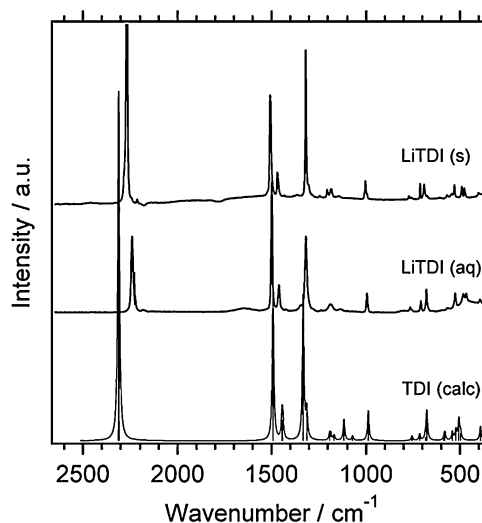


**Fig. 2** Experimental Raman spectra of the LiTDI salt (top) and a 1 M LiTDI:H$_2$O electrolyte (middle), compared with a calculated spectrum of TDI ($C_s$-symmetry; B3LYP/6-311+G(d)).

solid LiTDI (top), a 1 M aqueous electrolyte (middle), and a calculated minimum energy vacuum structure[6] of the TDI anion (bottom) are presented. The solid salt represents an environment where the anion is strongly coordinated to Li^{+}, while the aqueous solution provides a clear Raman spectrum of "free" anions in solution; the high dielectric constant of water implies that the ions are effectively screened from each other and, in addition, there is limited anion and solvent band overlap. Comparing the experimental spectra shown in Fig. 2, the overall appearance is very much the same. The most pronounced change is the band position of the stretching mode of the cyano group, $\nu$(C3–N2), which is located at ~2267 or ~2238 cm$^{-1}$ in the salt and aqueous electrolyte, respectively.

The calculated Raman spectrum of TDI is in good agreement with the experimental, and is used to assign the TDI normal modes (Table 2 and Table S1, ESI†). Of the 33 normal modes of TDI—all Raman active and non-degenerate—approximately 20 are identified experimentally. The calculated Raman spectrum is treated in more detail in Section 3.3.

11138 | *Phys. Chem. Chem. Phys.*, 2011, **13**, 11136–11147

This journal is © the Owner Societies 2011

**Table 2** Assignment of selected vibrational modes of TDI (B3LYP/6-311 + G(d)). Experimental data are for the 1 M LiTDI:$H_2O$ electrolyte. A complete assignment is available in Table S1, ESI†

| $\nu_{exp}$/cm$^{-1}$ | $\nu_{calc}$/cm$^{-1}$ | IR$_{Int}$/km mol$^{-1}$ | $R_{Act}$/Å$^4$ amu$^{-1}$ | Tentative assignment |
|---|---|---|---|---|
| 2238 | 2311 | 136 | 565 | $\nu_s$(C3–N2) |
| 1499 | 1492 | 63 | 149 | $\nu$(C4–C1; C2–C2*) |
| 1317 | 1331 | 44 | 124 | $\nu_{as}$(N1–C2) |
| 996 | 988 | 92 | 16 | $\delta$(N1–C1–N1*) |

Based on the observed mode intensities and the local separation of modes, several suitable regions exist for the characterization of TDI: the high intensity band located approximately between 2300 and 2200 cm$^{-1}$, a region of medium to strong intensity bands at 1600–1200 cm$^{-1}$, and a region of weak intensity bands at lower wavenumbers, <1200 cm$^{-1}$. The bands of these regions are explored further and commented in terms of solvent properties and electrolyte component interactions.

**Solvent and coordination effects.** The sensitivity of cyano group stretching vibrations to the surrounding is well documented[26] and has frequently been used to study ion–ion and ion–solvent interactions.[11,27–31] Here, at ~2200 cm$^{-1}$, the $\nu$(C3–N2) signature of TDI varies over 14 cm$^{-1}$ between electrolytes (Fig. 3a) and is clearly separated in all but the ACN-based electrolytes. Also, its position as a function of solvent properties ($\varepsilon$, AN, and DN; Table 1) is found to correlate strongly with the solvent AN (not shown). This is not surprising, since the AN is a measure of the Lewis acidity of the solvent; here the ability of the solvent molecules to accept the lone pair electrons on the cyano group nitrogen of TDI—the Lewis base.

Taking into account the fact that the solvents are also Lewis bases to different extents suggests that a stronger Lewis base (high DN) would be more resistant towards accepting electron density from the anion. Results, accordingly, are obtained by the excellent fit of the $\nu$(C3–N2) shift with respect to the ratio AN/DN (Fig. 3b).

More subtle changes in the shape and width of the $\nu$(C3–N2) band indicate an envelope of contributing bands (Fig. 3a), possibly from Li$^+$–TDI associations. However, in these systems the $\nu$(C3–N2) mode is foremost a sensitive probe of the solvent acceptor/donor properties.

At wavenumbers <1600 cm$^{-1}$ other features accompany the systematic changes in the band position with AN/DN. For the LiTDI:ACN and LiTDI:ACT electrolytes additional bands are resolved—a sign of direct association of TDI, possibly with Li$^+$. In the 1600–1200 cm$^{-1}$ region of these electrolytes, two components, $\Delta\nu \approx$ 4–8 cm$^{-1}$, are seen for each of the $\nu$(C4–C1; C2–C2*) and $\nu_{as}$(C1–N1) modes at ~1500 and ~1300 cm$^{-1}$, respectively (Fig. 3c and d; Table 2). For the remaining electrolytes no band splits are seen in the cases where the TDI modes are clearly resolved (Fig. 3c). In the LiTDI:TGL electrolyte, solvent signatures prevent a clean observation of the $\nu$(C4–C1; C2–C2*) and $\nu_{as}$(C1–N1) modes, however, the positions of these bands are still easily identified at ~1486 cm$^{-1}$ and ~1304 cm$^{-1}$ (Fig. 4c). Hence, the maximum band shifts from water to TGL electrolytes (~13 cm$^{-1}$) are of the same magnitude as for the $\nu$(C3–N2) mode (~14 cm$^{-1}$),



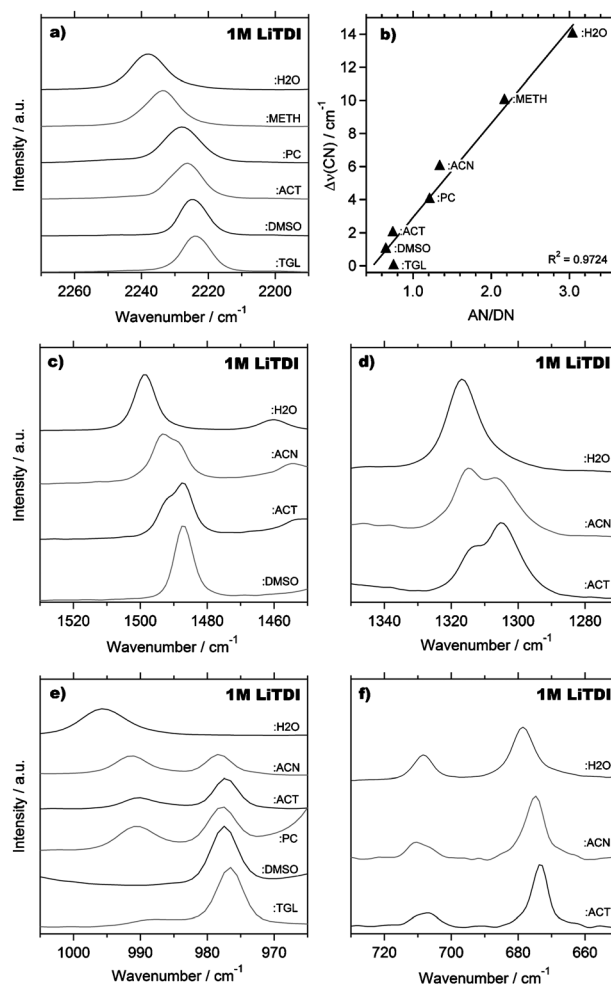**Fig. 3** Raman spectra of 1 M LiTDI electrolytes; (a) highlighted $\nu$(C3–N2) region, (b) correlation of the position of the $\nu$(C3–N2) band maxima with the ratio of the solvent AN and DN (Table 1), (c) the $\nu$(C4–C1; C2–C2*) mode, (d) the $\nu_{as}$(N1–C2) mode, (e) the $\delta$(N1–C1–N1*) mode, and (f) selected low wavenumber modes.

indicating an equally strong solvent dependence for all three modes. However, the added benefit of the $\nu$(C4–C1; C2–C2*) and $\nu$(C1–N1) modes is their sensitivity to the immediate environment of the anion, making them useful as probes of ion–ion interactions.

For Raman shifts <1200 cm$^{-1}$, the $\delta$(N1–C1–N1*) mode just below 1000 cm$^{-1}$ is a promising band for analysis (Fig. 3e). This mode splits into two main components in ACN, ACT, and PC and is more clearly resolved ($\Delta\nu \approx$ 13 cm$^{-1}$) than in the 1600–1200 cm$^{-1}$ region. A similar enhancement effect is reflected also in the maximum difference in band positions (~19 cm$^{-1}$) between the aqueous and TGL electrolytes. Thus, the $\delta$(N1–C1–N1*) mode is identified as the most sensitive probe of the surroundings of TDI overall.

Vibrational modes at lower wavenumbers are either less sensitive to the specific electrolyte or of weak intensity (Fig. 3f), and are therefore given less attention.

**LiTDI concentration effects.** The split TDI modes at ~1500, ~1300, and ~1000 cm$^{-1}$ indicate at least two different environments of the anion in these electrolytes. We here focus
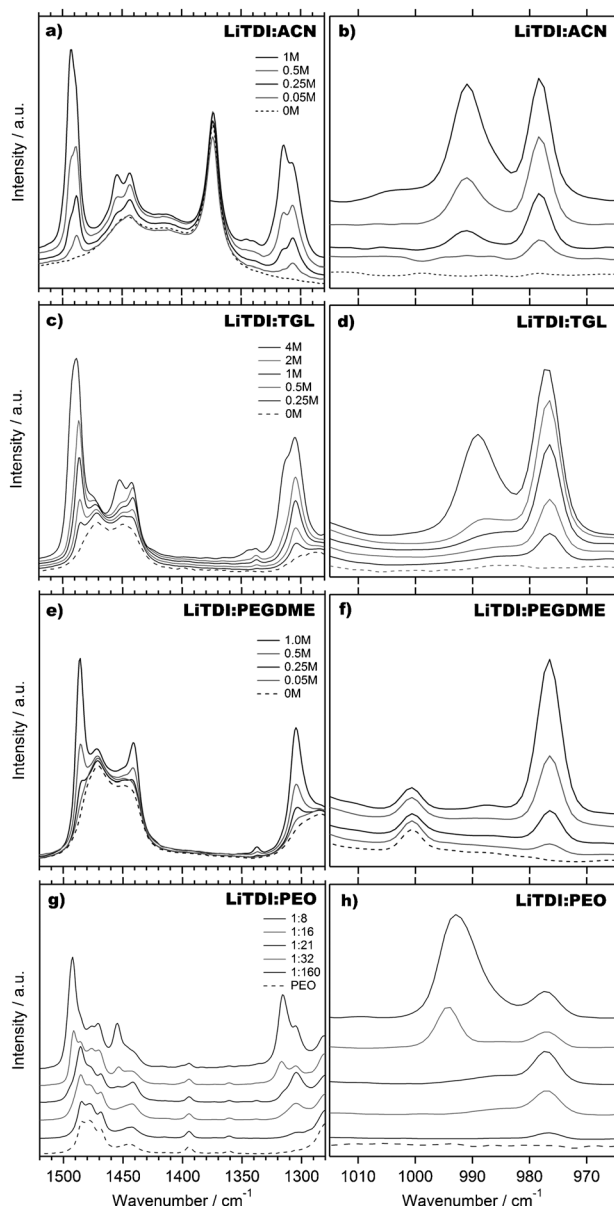
**Fig. 4** Raman spectra showing the salt concentration dependence of LiTDI electrolytes based on ACN (a and b), TGL (c and d), PEGDME (e and f), and PEO (g and h).

our analysis on the LiTDI concentration dependence of these modes in ACN and three polymer electrolytes; two liquid (TGL, PEGDME) and one solid (PEO).

In ACN the formation of associates is very favourable as the intensities of the high wavenumber components increase rapidly with LiTDI concentration (Fig. 4a and b). In the most concentrated ACN electrolyte, even a third band emerges ($\sim 1005$ cm$^{-1}$), indicating the formation of further, structurally different, associates.

In the polymer electrolytes, on the other hand, the strong coordination of alkali ions by the ether oxygen atoms[32,33] promotes salt dissociation, despite the low AN/DN and permittivity solvents. In the Raman spectra of $\leq 4$ M LiTDI:TGL electrolytes, pronounced changes with concentration are seen only in the most concentrated electrolyte (Fig. 4c and d).

No signs of associates are found for the less concentrated $\leq 1$ M electrolytes of LiTDI:PEGDME—neither in any of the analyzed regions in this work (Fig. 4e and f), nor in a previous Raman spectroscopic study of the $\nu$(C3–N2) mode of TDI.[4] The observed onset of aggregation effects in the TGL electrolyte is a reference for the PEO-based SPEs. However, a direct comparison of salt concentration between the liquid and solid electrolytes requires a more suitable unit, such as lithium ions per oxygen atom (Li : O). In these units the 4 M LiTDI:TGL and 1 M LiTDI:PEGDME electrolytes translate to $\sim 1 : 6$ and $\sim 1 : 24$ Li : O, respectively.

In the SPEs, the onset of anion association effects is observed at lower concentrations compared to the liquid TGL electrolytes. In the investigated concentration range of SPEs, 1 : 160 to 1 : 8, qualitative differences in the Raman spectra with concentration are apparent between 1 : 21 and 1 : 16.

In the 1 : 16 SPE, intensity is drastically shifted into the high wavenumber components of the probed bands (Fig. 4g and h), and in the 1 : 8 SPE these differences are further accentuated by the appearance of additional features. These new features include a band component at 680 cm$^{-1}$ and a multi-component band centered at $\sim 2250$ cm$^{-1}$, both of which are present also in the 1 : 6 TGL electrolyte—albeit less intense (neither of these bands are shown). Hence, qualitatively the results in the model oligoether electrolytes and the SPEs are similar with the difference that, at comparable concentrations, the association effects are stronger in the SPE. In part, this difference can be attributed to kinetic effects and multiple phases in the SPEs, as indicated by structural relaxations in the SPEs upon storage (see below).

**Ion–solvent interactions.** The evolution of TDI-bands observed with increasing salt concentration in the previous section is naturally attributed to Li$^+$–TDI interactions. However, as exemplified for TGL and PEGDME, ion–solvent interactions are also of importance. It is for example well known that cations with high polarizing power ($Z/r$), such as Li$^+$, impose well defined, and spectroscopically identifiable, local ordering of solvent molecules.[34] There is, for example, a consensus about the four-fold coordination of Li$^+$ in water[35,36] and ACN.[29,37,38] In polyether electrolytes the situation is a little more complex, since the exact coordination number depends on the number of repeating units, salt concentration, and type of anion (see discussion of Mao *et al.*).[39] In general, a Li$^+$ coordination number of four is expected only for TGL;[40] when the number of oxygen atoms increases there are strong computational[41–43] and experimental[39,44] indications of a preferential Li$^+$ coordination number of five or six.

In LiTDI:ACN electrolytes, the Li$^+$–ACN interactions are easily identified through shifts of the $\nu$(CC) + $\nu$(CH$_3$) combination band of ACN (2292 $\rightarrow$ $\sim 2305$ cm$^{-1}$), the $\nu$(CN) (2252 $\rightarrow$ $\sim 2275$ cm$^{-1}$), $\nu$(CC) (918 $\rightarrow$ $\sim 929$ cm$^{-1}$), and $\nu$(CCN) (379 $\rightarrow$ $\sim 390$ cm$^{-1}$) modes (Fig. S1a–c, ESI†). These results are in agreement with numerous previous detailed reports on Li$^+$ induced shifts of ACN modes.[27,28,31,37,38]

In the TGL and PEGDME electrolytes, as well as the SPEs, Li$^+$ solvation involves conformational changes in the oligomer/polymer backbone, which is reflected in the Raman spectrum in the 900–800 cm$^{-1}$ region.[38,45–47] The most clear change in
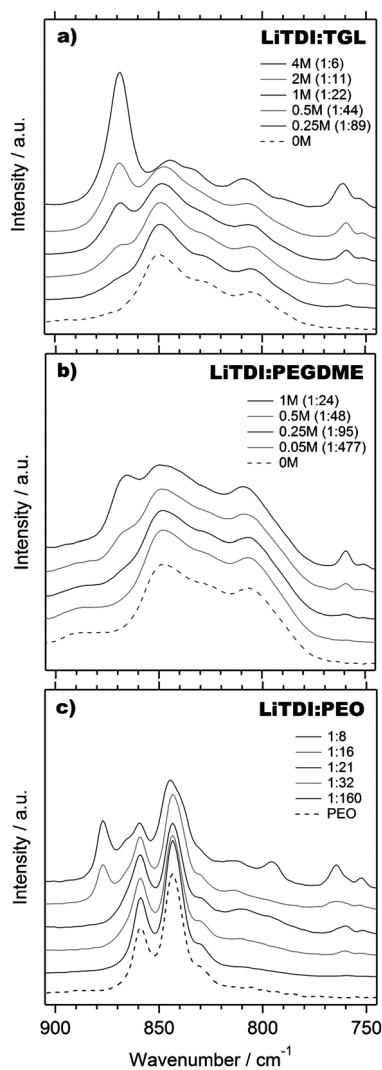
**Fig. 5** Raman spectra of LiTDI:polyether electrolytes showing Li$^+$ solvation effects on the vibrational modes of (a) TGL, (b) PEGDME, and (c) PEO.

the TGL and PEGDME electrolytes (Fig. 5a and b) is the appearance of a band at $\sim$870 cm$^{-1}$, already at low salt concentrations. In the SPEs (Fig. 5c) a strong band at $\sim$877 cm$^{-1}$—present only in the 1:8 and 1:16 electrolytes—is more pronounced compared to a weak shoulder at $\sim$863 cm$^{-1}$. The latter is present in all but the 1:160 SPEs, however, in the 1:21 and 1:32 SPEs, only as a broadening of the polymer band at $\sim$859 cm$^{-1}$. Brodin and Jacobsson[46] reported a strong polymer mode at $\sim$869 cm$^{-1}$ in crystalline LiCF$_3$SO$_3$:PEO (1:3) electrolytes, assigned to a Li$^+$ induced shift of the $\sim$860 cm$^{-1}$ combined rocking, $r$(CH$_2$), and $\nu$(COC) modes of crystalline PEO, with the polymer backbone (O–C–C–O) in a *trans–gauche–trans* (tgt) conformation.[48] The $\sim$869 cm$^{-1}$ mode was also identified by Brodin and Jacobsson in a non-stoichiometric complex of LiCF$_3$SO$_3$:PEO (1:9), with local intensity variations reflecting the composition and orientation of crystalline and amorphous regions at different probe volumes.[46] In the LiTDI-based SPEs reported here, the band at 877 cm$^{-1}$ is shifted substantially both with respect to the $\sim$860 cm$^{-1}$ mode of pure PEO and

the $\sim$869 cm$^{-1}$ mode of LiCF$_3$SO$_3$:PEO. The position of the $\sim$877 cm$^{-1}$ band and its correlated appearance with the onset of TDI association effects between the 1:21 and 1:16 SPEs suggest that the anion has an important effect on the polymer backbone conformation, when present in the coordination sphere of Li$^+$.

In contrast to specific Li$^+$–solvent interactions, the formation of distinct stoichiometric TDI–solvent species is much less likely, because of the less polarizing polyatomic anion. In ACN-based electrolytes, the smaller anions of LiBr and LiI are known to modify the $\nu$(CH) (2942 cm$^{-1}$) mode of ACN considerably,[27,49] but no such effects are seen with larger anions such as ClO$_4^{-}$ [27] or TDI (not shown). Nevertheless, between protic and aprotic electrolytes the spectra of polyatomic anions can change considerably, which already has been demonstrated for TDI (Fig. 3). This raises important questions about the effect of water on the immediate surroundings of Li$^+$ and TDI in different electrolytes.

### 3.2 On the role of water in LiTDI electrolytes

**Influence of water on the spectra of ACN-based electrolytes.** Investigating potential effects of water on the spectra of LiTDI electrolytes is crucial, since water is introduced with the lithium salt, in trace or stoichiometric amounts, and may alter the TDI spectra—also in aprotic electrolytes.

Related to the LiTDI:ACN electrolytes, several vibration spectroscopic studies exist on mixtures of water and ACN—in the presence of a lithium salt[49,50] or without.[51,52] With two solvents present there is inevitably a competition between the solvents, first and foremost for solvating Li$^+$, but preferential anion solvation is sometimes also observed.[49] Using Raman spectroscopy and NMR, Keil *et al.*[50] investigated LiClO$_4$ solvation, in mixtures of ACN/H$_2$O. They concluded that Li$^+$ is preferentially solvated by water and with a coordination number of four, in support of earlier findings.

Given the ACN/H$_2$O mixtures prepared in this work, with a mole fraction of ACN $>0.25$, the effects of water on the ACN modes are in accordance with previous results;[51] for the LiTDI electrolytes a broadening and slight shift ($\leq$3 cm$^{-1}$) of free ACN bands to higher wavenumbers is seen with increased water content. However, more drastic changes are seen for the Li$^+$ coordinated ACN bands, due to the competition for Li$^+$. Keil *et al.* reported that for molar ratios of four or more water molecules to one Li$^+$ ion, the Raman signature of the Li$^+$ coordinated $\nu$(CN) mode of ACN is absent.[50] In the LiTDI electrolytes the corresponding signature disappears *almost* completely between water to Li$^+$ ratios of 1/3 and 1/11 (Fig. S1d–f, ESI†), which corresponds to the electrolytes prepared from lithium salt containing crystal water and the first direct addition of water, respectively. Thus, the small amount of water introduced with the salt is not enough to cause a significant change of the Li$^+$ environment. However, more surprising is the weak signal of Li$^+$ coordinated ACN at $\sim$2275 cm$^{-1}$ that remains in the spectrum of the 1:11:20 (Li:H$_2$O:ACN) electrolyte—shifted to slightly lower wavenumbers (inset in Fig. S1d, ESI†). Apparently, there is still some Li$^+$–ACN association in this electrolyte.

The effect of water on the TDI modes is more dramatic compared to the ACN modes (Fig. 6). For the

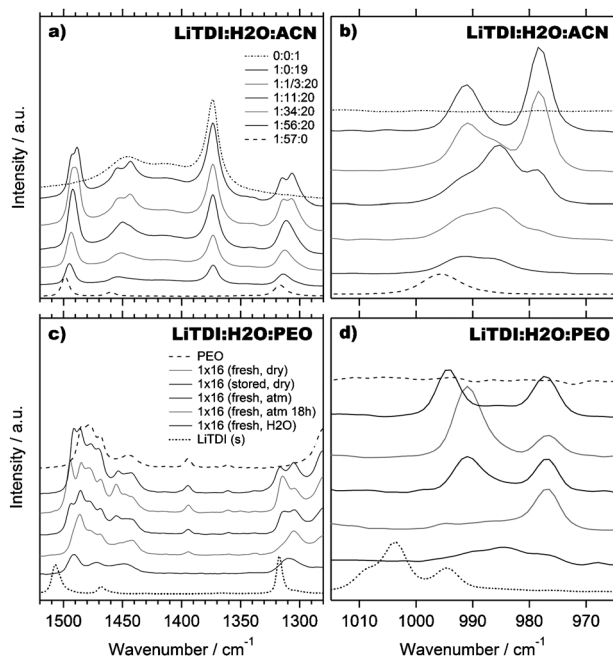**Fig. 6** Raman spectra showing the effect of water on the TDI modes in (a and b) ACN-based electrolytes and (c and d) PEO-based electrolytes.

$\nu$(C4–C1; C2–C2*) and $\nu_{as}$(C1–N1) modes, at $\sim$1500 cm$^{-1}$ and $\sim$1300 cm$^{-1}$, respectively, the effects are similar; the two well resolved band components of each mode merge into a single band (Fig. 6a). With the water content further increased, the band maximum moves towards higher wavenumbers. In the 1:56:20 electrolyte, where the Li$^+$ to solvent ratio coincides with that of each single solvent system (LiTDI:H$_2$O $\approx$ 1:57 and LiTDI:ACN $\approx$ 1:19), the $\nu$(C4–C1; C2–C2*) band at $\sim$1495 cm$^{-1}$ is shifted $+$6 cm$^{-1}$ with respect to the low wavenumber component in the water-free electrolyte (1:0:19), and $-$4 cm$^{-1}$ with respect to the ACN-free electrolyte (1:57:0). Similar magnitudes of shifts are seen for the $\nu_{as}$(C1–N1) mode.

Most clear are the changes at $\sim$1000 cm$^{-1}$, where the two components of the $\delta$(N1–C1–N1*) mode in the water-free electrolyte become three, as water is introduced with the salt (Fig. 6b). Although a two component description may be valid for the water-free sample, for which each component can be fitted with a single Voigt function, three components in the water containing samples is most certainly a too simple description.

Yet, with increasing water concentration the new component becomes the dominant feature of the 1:11:20 electrolyte at the expense of both initial components. In the 1:56:20 electrolyte the intensity has been redistributed so that the maxima of the center and high wavenumber components are of equal intensities, while the intensity of the low wavenumber component is negligible.

A possible origin of the third component of the $\delta$(N1–C1–N1*) mode, emerging in the mixed solvent electrolyte, is a change of the first solvation shell of TDI, from ACN to water. Comparing the position of this band with the position of the corresponding band of the aqueous electrolyte, the

former is obviously influenced by the presence of a second solvent and moves towards higher wavenumber as the water concentration increases. However, this does not seem to be true for the ACN solvated TDI mode—the peak position of which is more or less constant with the added water. Moreover, the high wavenumber component remains with increasing water content, suggesting that the corresponding complexes or associates keep their integrity, despite the solvating power of water. A similar conclusion can be drawn from the observation that signs of a Li$^+$–ACN band is still present in the 1:11:20 electrolyte.

**SPEs—effects of storing and atmospheric exposure.** A different and more subtle approach for introducing water into electrolytes is to expose SPEs to the atmosphere and record consecutive Raman spectra as a function of time. For this purpose a second 1:16 SPE was cast, part of which was stored in a sealed container in a dry box for twelve weeks. The Raman spectrum of the fresh 1:16 SPE (Fig. 6c and d) shows the same qualitative features as the 1:16 SPE in Fig. 4, however, upon storage the SPE undergoes significant reorganization. The $\nu$(C3–N2) mode, little affected in the fresh sample, is in the spectrum of the stored sample split into two band envelopes (Fig. S2, ESI†). The Raman spectrum of the solid salt shows that none of the envelopes in the stored 1:16 SPE can be attributed to salting out. Signatures of the reorganization of the stored SPE, with respect to the fresh SPE, are reflected throughout the spectrum, in particular the relative shift of the high wavenumber component at $\sim$1000 cm$^{-1}$ (Fig. 6d) and the absence of the $\sim$877 cm$^{-1}$ band (Fig. S2b, ESI†) are noted.

Atmospheric exposure of the SPE immediately leads to minor changes, however, the changes observed after 18 hours are more significant; the anion association has relaxed, and there are only minor signs of split TDI modes (Fig. 6c and d). After soaking the SPE with a drop of water the sign of a crystalline PEO phase at $\sim$859 cm$^{-1}$ is lost (Fig. S2b, ESI†) and the effects on the $\delta$(N1–C1–N1*) mode (Fig. 6d) are comparable to the effect of water on the ACN-based electrolytes.

To address the effects of atmospheric exposure on less concentrated and fresh SPEs, Raman spectra of a 1:21 SPE were recorded before and after contact with atmosphere. Changes between these spectra are concentrated mainly to the $\delta$(N1–C1–N1*) mode, and are immediate (not shown); in the first recording after atmospheric exposure, a second TDI component at $\sim$991 cm$^{-1}$ disappears and in its place a broader feature appears at $\sim$985 cm$^{-1}$ (see Fig. 4h). After this initial change, no further changes are observed with time. Comparing the spectra of the $\delta$(N1–C1–N1*) mode in Fig. 6b and d, the positions of the discrete components correlate very well between the ACN electrolytes and the stored 1:16 SPEs (also the dry 1:21 SPE); in the water-free electrolytes the low and high wavenumber components are positioned at $\sim$977–978 cm$^{-1}$ and $\sim$991 cm$^{-1}$, respectively, and upon addition/absorption of water an intermediate component appears, approximately centered between the former. The difference between the liquid and solid electrolytes is that, in the SPEs, the intermediate component grows at the expense of

the high wavenumber component, which is lost. Hence, in the SPEs these features are consistent with the interpretation of associate dissolution with absorbed water and the formation of water solvated anions, as recognized by the growing intermediate component.

We conclude that for the SPEs investigated in this work, Raman spectra recorded in atmosphere, immediately after exposure (1:8 → 1:160, Fig. 4g and h) are expected to be altered slightly by the exposure—in the qualitative direction of the less concentrated samples. The effects on the $\delta$(N1–C1–N1*) mode are clear, and found to be immediate for low salt concentration SPEs ($\leq$1:21)—within the sampling time of a Raman spectrum. However, for the more concentrated SPEs ($\geq$1:16), the spectral changes at atmospheric exposure are slower. For the 1:8 and 1:16 SPEs in Fig. 4 (exposed to atmosphere) and the fresh, dry 1:16 electrolyte in Fig. 6, the position of the high wavenumber component ($\sim$995 cm$^{-1}$) indicates that the associates of these electrolytes are structurally different from the low concentration SPEs ($\sim$990 cm$^{-1}$), differences which are in part lost upon SPE storage (Fig. 6d, $\sim$994 → $\sim$991 cm$^{-1}$).

### 3.3 Computational modeling of TDI associates

**Anion band assignment.** Significant association of the TDI anion is seen in the ACN- and PEO-based electrolytes, especially with increasing LiTDI concentration. To aid the interpretation of the local structure, vibration spectra are computed for simple associates; with both ion–ion and ion–solvent interactions taken into account. An assignment of normal modes for TDI and of the nomenclature used is introduced in Table 2 and Fig. 1, respectively. The experimentally observed vibrations identified as promising probes of TDI associates are assigned to the calculated modes at 1492, 1331, and 988 cm$^{-1}$, the $\nu$(C3–C1; C2–C2*), $\nu_{as}$(C1–N1), and $\delta$(N1–C1–N1*) modes, respectively. Although the assignment of the first and last of these is straightforward, due to the clear separation of the $\sim$1500 and $\sim$1460 cm$^{-1}$ modes and the absence of bands close to 1000 cm$^{-1}$, the assignment of the $\sim$1300 cm$^{-1}$ mode is non-trivial. A closer inspection of the most intense $\sim$1300 cm$^{-1}$ mode in the aqueous reference spectrum shown in Fig. 2 and the liquid electrolyte spectra shown in Fig. 4 reveals a high wavenumber component to the most intense band, at $\sim$1350–1330 cm$^{-1}$, suggesting that the predicted relative Raman activities for the two calculated modes at 1331 and 1312 cm$^{-1}$ are wrong (Table S1, ESI†). However, the asymmetry of the strong $\sim$1300 cm$^{-1}$ band of the aqueous electrolyte (Fig. 3d)—indicative of an unresolved weak intensity component at lower wavenumbers—together with the low wavenumber shoulder observed in the solid salt spectrum (Fig. 2) are both in good agreement with the "narrow" ($<$20 cm$^{-1}$) calculated separation and the predicted relative activities (Table S1, ESI†). Hence, the experimental response at $\sim$1340 cm$^{-1}$ is most likely a non-fundamental mode, possibly an overtone of the $\sim$680 cm$^{-1}$ mode.

A comment regarding two calculated weak and medium intensity modes at 1073 and 1118 cm$^{-1}$ (Table S2, ESI†) is warranted, since no experimental counterparts of these modes are observed. They represent isolated motions of the
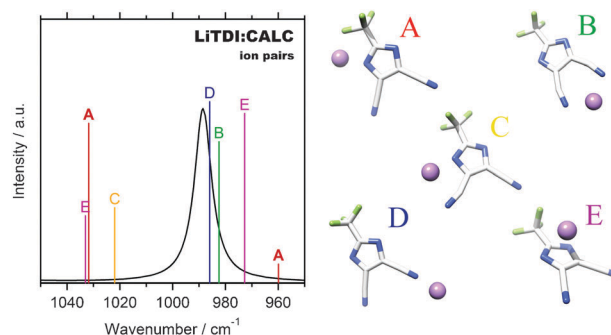


**Fig. 7** Comparison of calculated Raman spectra of the $\delta$(N1–C1–N1*) mode for Li$^+$:TDI ion pairs (A–E, vertical lines) and TDI (envelope). The ion pairs are represented without envelopes for ease of visualization.

fluoroalkyl carbon (C4) in or out of the plane of the anion, modes unlikely to be important in solution. Thus, the high wavenumber component of the $\sim$1000 cm$^{-1}$ mode is unlikely to originate from these modes, despite being the nearest neighbors.

**Ion pairs.** In previous work, four stable Li$^+$ coordinated ion pair configurations were reported for TDI,[6] and in the course of this work a fifth configuration was found.§ Together these ion pairs (Fig. 7, A–E) offer the simplest models of TDI associates in the LiTDI electrolytes; Li$^+$ has only translational degrees of freedom and no surrounding solvent molecules are included. Consequently, exaggerated perturbations of the TDI modes are expected as no charge screening can occur. However, important qualitative information can be extracted, such as the direction and relative magnitude of shifts, to discriminate between possible ion pair configurations in real electrolytes.

The ion pair structures shown in Fig. 7 are identified by letters in order of decreasing interaction energy, A to E.[6]

Out of the five ion pairs, only the most stable configuration (A) reproduces the experimentally observed directions of shifts for all four modes, without significant contributions in the "wrong" direction (Fig. S3, ESI†). The Raman response of the ion pairs (vertical lines) with respect to the TDI signature (envelope) is exemplified for the $\delta$(N1–C1–N1*) mode in Fig. 7.

In A, Li$^+$ coordinates with TDI in the plane of the imidazole ring, interacting bidentately with the ring nitrogen atom and a fluoro atom. Thus, as previously observed also for LiPATC,[53] use of ion pair models gives a congruent picture both in terms of interaction energy and spectral changes.

**Solvated ion pairs.** In the idealized ion pair description the lithium ion is often restricted to a coordination number of maximum two. However, in the presence of a solvent Li$^+$ can acquire a higher coordination number, such as the aforementioned four-fold coordination in ACN, water, or mixtures thereof. To investigate the effects of an increased coordination number on the normal modes, Raman intensities, and geometry of ion pair configuration A, up to three solvent molecules

---

§ LiTDI (C); $E_{diss} = (E_{Li+} + E_{TDI}) - E_{ion\ pair} = 492$ kJ mol$^{-1}$ [B3LYP/6-311+G(d)].

Explicitly solvated ion pairs



Vacuum multiplets

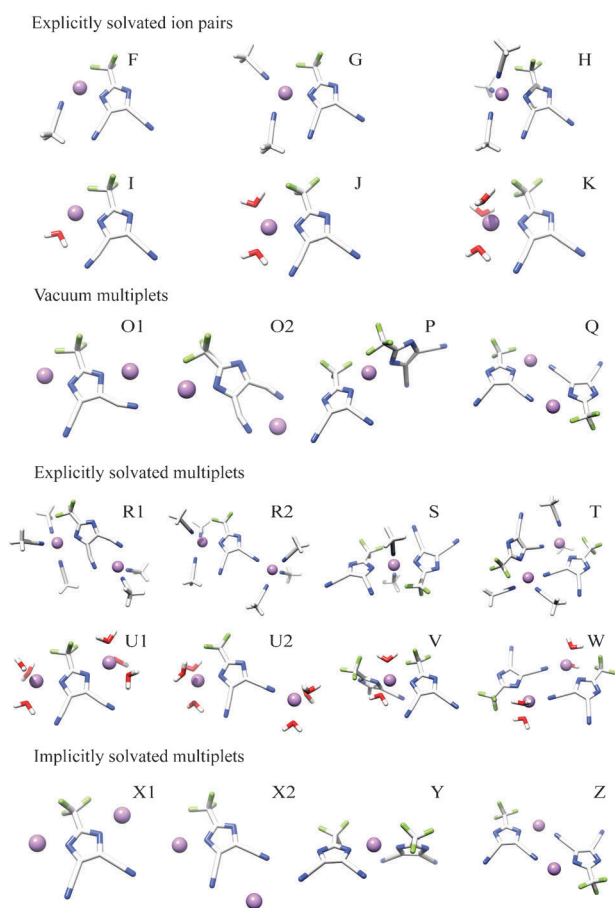Explicitly solvated multiplets

Implicitly solvated multiplets

**Fig. 8** Calculated structures of explicitly solvated LiTDI ion pairs, F–K, vacuum and solvated multiplets, O1–Z.

(ACN or H$_2$O) were added explicitly to A, to give the solvated ion pair configurations F–H and I–K, respectively (Fig. 8).

Compared with the non-solvated ion pair, the minimum distance between Li$^+$ and TDI is increased in all solvated structures, the Li–N1–C2 angle is decreased (Table S2, ESI†), and effectively the coordination to the fluoroalkyl group loses its significance. This challenges the coordinating role previously assigned to the fluoroalkyl group of imidazolides and benzimidazolides.[6] It is also notable that when three solvent molecules are added explicitly to the most stable vacuum ion pair, Li$^+$ relaxes into a four-coordinated complex, despite the opportunity of being five-coordinated.

In the case of ACN the structural changes are systematic, as the number of solvent molecules increases. The trend in shifts of the $\nu$(C4–C1; C2–C2*), $\nu_{as}$(C1–N1), and $\delta$(N1–C1–N1*) normal modes is almost as systematic; for the first two modes the shifts decrease between each complex, from +17 and +35 cm$^{-1}$ in the non-solvated ion pair to +9 and +14 cm$^{-1}$ in the LiTDI(ACN)$_3$ complex. For the third mode there is an initial increase in shift between the non-solvated ion pair and the mono-solvated complex, however, with a second solvent molecule a much more reasonable value is obtained, and in LiTDI(ACN)$_3$, the predicted shift of +12 cm$^{-1}$ is very close to the experimental value of +13 cm$^{-1}$. For the water-solvated ion pairs, LiTDI(H$_2$O)$_{1-3}$, the overall trends are similar to the ACN-solvated models, however, there are a

few exceptions; the most notable being the increased shift of the $\nu$(C4–C1; C2–C2*) mode in the solvated compared to the non-solvated ion pair. A 10 cm$^{-1}$ difference in shift for this mode between the LiTDI(H$_2$O)$_3$ and LiTDI(ACN)$_3$ complexes has its origin in the association of two water molecules to the fluoroalkyl group of the former.

From the latter result and the solvated ion pair structures shown in Fig. 8 in general, interactions between the solvent molecules and TDI are apparent. These interactions are in part responsible for the differences between the ACN and water solvated complexes, but as argued for the non-solvated ion pair, these interactions may be exaggerated, since there is no outer shell damping the effects. Hence, the description of the Li$^+$–TDI coordination is improved by adding a first explicit solvation "shell", but the effects of a second, third, ... solvation shell are still unaccounted for.

An alternative to the explicit modeling of solvent effects is to account for the solvent implicitly via electrostatic effects. In a recent study of complexation energies of Li$^+$ in ACN,[54] implicit modeling was found to give results comparable to explicit models. In Table S3 (ESI†) the results of such an implicit continuum approach are included as LiTDI$_{ACN}$ and LiTDI$_{H_2O}$, respectively. Comparing the implicit LiTDI$_{ACN}$ and explicit LiTDI(ACN)$_3$ results, the structural parameters of both models are very similar, but the implicit model reproduces the experimental shifts of the ~1500 and ~1300 cm$^{-1}$ modes better [$\Delta\nu_{exp}$ = +4 and +8 cm$^{-1}$; $\Delta\nu_{calc}$ = +7 and +9 cm$^{-1}$ (LiTDI$_{ACN}$); +9 and +14 cm$^{-1}$ (LiTDI(ACN)$_3$)].

A weakness of the continuum approach is revealed when comparing the results for LiTDI$_{ACN}$ and LiTDI$_{H_2O}$; the Raman spectra of these models are close to identical. From experiments there are no or very few ion pairs in the aqueous electrolyte, implying in one sense that the modeling of an ion pair in water is an incorrect Ansatz. However, also the calculated spectra for the implicitly solvated anions TDI$_{H_2O}$ and TDI$_{ACN}$ are almost identical. This is far from the experimental situation where the free anion bands are shifted substantially between the aqueous and ACN-based electrolytes. An electrostatic continuum description would therefore not be a suitable model for the solvent dependence of the anion bands, but neither is an experimental description in terms of the relative permittivity of solvents.

In summary, both the explicit and implicit models have strengths and weaknesses in addressing the ion–solvent interactions. Overall they both offer shifts mainly in correlation with experimental observations. In an attempt to possibly reach even further, combining the two approaches for ion pair A, with an inner coordination sphere of water and an implicit ACN surrounding, LiTDI[3H$_2$O]$_{ACN}$ (Table S2, ESI†), leads to large changes compared to the corresponding explicit only model, but only minor systematic changes compared to the implicit solvation. Thus, the implicit effects clearly dominate over the explicit. With respect to the experimental results the combined approach offers little or no improvement compared to the implicit model. Hence, the best compromise is to invoke the implicit models for better magnitudes of spectral shifts, and the explicit for an analysis of specific interactions between solvent and solute—although these should be expected to be exaggerated.

11144 | *Phys. Chem. Chem. Phys.*, 2011, **13**, 11136–11147

This journal is © the Owner Societies 2011

**Ion associates beyond ion pairs.** With increasing concentration there is an increased probability of larger associates being formed, especially in the ACN-electrolytes. The large splitting of the band at $\sim 1000$ cm$^{-1}$, the width and apparent asymmetry of the high wavenumber component, as well as the shoulder appearing at yet higher wavenumbers (Fig. 4b); all together suggest that a number of different associates contribute to this component. Here structures and Raman spectra of three larger TDI associates ([Li$_2$TDI]$^+$, [Li(TDI)$_2$]$^-$, and Li$_2$TDI$_2$) are presented: in vacuum, O–Q; in explicit, R–W; and implicit, X–Z, solvated forms (Fig. 8, Table S2, ESI†). With the $\delta$(N1–C1–N1*) mode as the most sensitive experimental signature and the mode that is best represented overall in the computed ion pair descriptions (most accurate shifts), we concentrate our discussion of larger associates to this mode. In Fig. 9a, the vacuum ion pair results (vertical lines) do not only show a wide spread around the TDI band (envelope), but the ion pair $\delta$(N1–C1–N1*) modes are split to a different extent, due to the coupling of this mode to the $\nu$(C–F) modes of the fluoroalkyl group. From the high wavenumber components originating from each model, the result is a clear separation of each type of associate; among the multiplets a $\sim 20$ cm$^{-1}$ increase in wavenumber is predicted between each model (Table S2, ESI†), going from the triplets Li(TDI)$_2$ (P), $\Delta\nu = +18$ cm$^{-1}$, and Li$_2$(TDI) (O2), $\Delta\nu = +38$ cm$^{-1}$, via the dimer Li$_2$(TDI)$_2$ (Q), $\Delta\nu = +58$ cm$^{-1}$, to the triplet Li$_2$(TDI) (O1), $\Delta\nu = +82$ cm$^{-1}$ (outside the window of Fig. 9a). In reference, the ion pair model (A) predicts a value intermediate that of O2 and Q.

In contrast, the overall appearances in Fig. 9b and c show that most of the explicitly and implicitly solvated ion associates give rise to bands at similar positions, shifted $+11$ to $+17$ cm$^{-1}$ from the free anion band—depending on the model. Also, the results from explicit ACN or H$_2$O solvation models are very similar (Table S2, ESI†), with the exception of structure V, where the water molecules are strongly associated with the fluoromethyl group of the anion. Different are the positions of the predicted bands of structures U1 and X1. In these structures two Li$^+$ coordination spheres can be imagined to share, or be bridged by, a common anion, with both of the imidazole nitrogen atoms as the bridging points. Although attempts to converge a corresponding explicit ACN solvated structure failed, it is reasonable to assume that such structures could also form in the ACN electrolyte, with the same qualitative change in the position of the $\delta$(N1–C1–N1*) band. Thus, the results of the solvated models (Fig. 9b and c) are in very good agreement with the experimental results of the LiTDI:ACN electrolytes (Fig. 4b); at low salt concentrations there are very few ion-associates, Li$^+$ has an all solvent coordination sphere, and the "free" anion band is dominating the highlighted part of the spectrum. With increasing salt concentration, one or possibly two anions are incorporated into the inner coordination shell of Li$^+$ to give a second band envelope, of potentially several unresolved associates, and in the most concentrated electrolyte there are indications, by the third band envelope at $\sim 1002$ cm$^{-1}$, of structures where one anion is shared symmetrically by two Li$^+$.
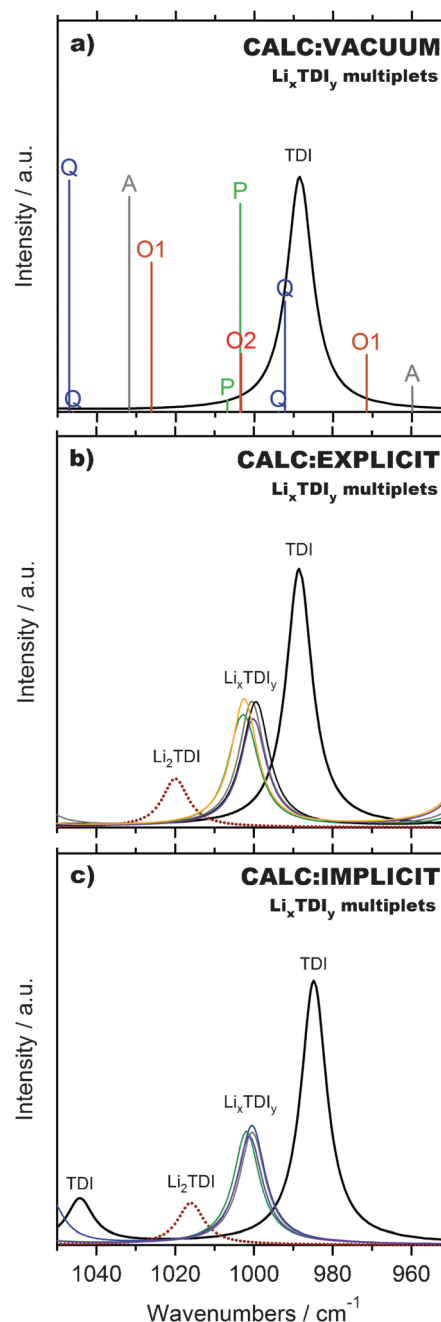


**Fig. 9** Simulated Raman spectra of Li$_x$TDI$_y$ associates (a) in vacuum, (b) explicitly solvated by ACN or H$_2$O, and (c) implicitly solvated by ACN. From high to low wavenumbers the structures responsible for the bands in (b) are U1, T, R1, R2, H, and S; in (c) X1, Z, Y, X2, and L. The intensities of the ion pair structures in (b) and (c) have been scaled by 0.5 or 0.2 to better reflect the experimental intensity distribution.

**TDI–solvent interactions.** Predictions of TDI band shifts due to different solvent environments (water or ACN) are not as straightforward as the ion–ion models. Implicit solvation, as presented for the ion pairs above, does not differentiate between water and ACN as solvents, and the construction of a realistic explicit solvation shell of the large TDI anion is difficult. However, the results of a very crude model, consisting

of 1 : 1 TDI : solvent pairs in configurations similar to those of ion pairs A and C (not shown), suggest two differences: (1) TDI:$H_2O$ pairs are more stable than TDI:ACN pairs, and (2) the shift of the $\delta$(N1–C1–N1*) band is larger for TDI:$H_2O$, $\sim$6–7 cm$^{-1}$, compared to $\sim$2–3 cm$^{-1}$ for TDI:ACN—the exact shift depends on the configuration.

Although such simple models do not offer quantitative results, the trends comply with experimental results, regarding the relative positions of the solvated TDI band in these solvents. Moreover, the interaction energies and shifts are small compared with the vacuum results for the corresponding Li$^+$:TDI ion pair, as expected from the different nature of the interactions—ion–ion or dipole–ion.

The above results relate to the introduction of water, but an important difference between the simple 1 : 1 models and the real electrolytes is the collective effect of many more solvent molecules coordinating to the anion. Experimentally we observe an $\sim$18 cm$^{-1}$ difference in the position of the $\delta$(N1–C1–N1*) band of the free anion between the aqueous and ACN electrolytes—an effect larger than that induced by ion pairing in the ACN electrolyte. However, in the mixed ACN/water electrolytes the band positions are intermediate to those of the single-solvent electrolytes and change smoothly with solvent ratio (Fig. 6a–b) and relative electrolyte permittivity, apart from an initial abrupt change in band positions at small $H_2O$/ACN ratios. This abrupt change is interpreted as preferential solvation of TDI by water, a situation where the simple ion–solvent models become relevant as the differences are concentrated to the nearest neighbours of the anion.

## 4. Conclusions

For spectroscopic analysis of LiTDI based electrolytes, the $\nu$(C3–N2) band of TDI is a sensitive probe of the solvent surrounding, but a poor probe of ion–ion interactions. In contrast, modes based in the imidazole ring: $\nu$(C4–C1; C2–C2*), $\nu_{as}$(N1–C2), and especially $\delta$(N1–C1–N1*), are found to be excellent choices to reveal ion association in for example LiTDI:ACN and LiTDI:PEO electrolytes.

DFT calculations using explicit and implicit solvated models suggest monodentate coordination between Li$^+$ and TDI, rather than the bidentate coordination favoured in vacuum. The result is a far better correspondence to all the experimental Raman spectra. For ionic aggregates beyond ion pairs the differences between the vacuum and solvated descriptions are further accentuated, emphasizing the importance of selecting the proper atomic DFT model(s).

Only by a detailed and combined Raman and DFT analysis of the $\delta$(N1–C1–N1*) mode can we predict TDI to coordinate to Li$^+$ via at least one imidazole nitrogen atom. Furthermore, only when both imidazole nitrogen atoms are symmetrically coordinated by two Li$^+$ does this band shift position significantly. The invariance of band positions for several associates makes it hard to differentiate among these solely on the basis of vibrational spectroscopy.

Addressing the role of water in LiTDI based electrolytes suggests preferential solvation of TDI by water from the observation of a new component of the $\delta$(N1–C1–N1*) mode,

an effect observed clearly only through direct addition of water or uptake of water upon electrolyte storage. Thus, a window for Raman analysis of electrolyte hydration is presented here.

The results of this work should be useful for further investigations, by spectroscopy or other techniques, for a qualitative—and possibly quantitative—analysis of the role of the local structure for practical application of LiTDI based electrolytes.

## Acknowledgements

## Notes and references

1 A. Hammami, N. Raymond and M. Armand, Nature, 2003, 424, 635.
2 C. L. Campion, W. T. Li and B. L. Lucht, J. Electrochem. Soc., 2005, 152, A2327.
3 N.-S. Choi, I. A. Profatilova, S.-S. Kim and E.-H. Song, Thermochim. Acta, 2008, 480, 10.
4 L. Niedzicki, M. Kasprzyk, K. Kuziak, G. Z. Zukowska, M. Armand, M. Bukowska, M. Marcinek, P. Szczecinski and W. Wieczorek, J. Power Sources, 2009, 192, 612.
5 L. Niedzicki, G. Z. Zukowska, M. Bukowska, P. Szczecinski, S. Grugeon, S. Laruelle, M. Armand, S. Panero, B. Scrosati, M. Marcinek and W. Wieczorek, Electrochim. Acta, 2010, 55, 1450.
6 J. Scheers, P. Johansson, P. Szczecinski, W. Wieczorek, M. Armand and P. Jacobsson, J. Power Sources, 2010, 195, 6081.
7 L. Niedzicki, M. Kaspzryk, K. Kuziak, G. Z. Żukowska, M. Marcinek, W. Wieczorek and M. Armand, J. Power Sources, 2011, 196, 1386.
8 M. Schmidt, U. Heider, A. Kuehner, R. Oesten, M. Jungnitz, N. Ignat'ev and P. Sartori, J. Power Sources, 2001, 97–98, 557.
9 J. S. Gnanaraj, M. D. Levi, Y. Gofer, D. Aurbach and M. Schmidt, J. Electrochem. Soc., 2003, 150, A445.
10 M. Egashira, B. Scrosati, M. Armand, S. Beranger and C. Michot, Electrochem. Solid-State Lett., 2003, 6, A71.
11 P. Johansson, S. Beranger, M. Armand, H. Nilsson and P. Jacobsson, Solid State Ionics, 2003, 156, 129.
12 M. Bukowska, J. Prejzner and P. Szczecinski, Pol. J. Chem., 2004, 78, 417.
13 L. Niedzicki, PhD thesis, Warsaw University of Technology, Warsaw, Poland, 2009.
14 C. Reichardt, Solvents and solvent effects in organic chemistry, Wiley-VCH, Cambridge, 2003.
15 V. Gutmann, G. Resch and W. Linert, Coord. Chem. Rev., 1982, 43, 133.
16 D. Brouillette, G. Perron and J. E. Desnoyers, J. Solution Chem., 1998, 27, 151.
17 W. Linert, Y. Fukuda and A. Camard, Coord. Chem. Rev., 2001, 218, 113.
18 M. J. Frisch, G. W. Trucks, H. B. Schlegel, G. E. Scuseria, M. A. Robb, J. R. Cheeseman, G. Scalmani, V. Barone, B. Mennucci, G. A. Petersson, H. Nakatsuji, M. Caricato, X. Li, H. P. Hratchian, A. F. Izmaylov, J. Bloino, G. Zheng, J. L. Sonnenberg, M. Hada, M. Ehara, K. Toyota, R. Fukuda, J. Hasegawa, M. Ishida, T. Nakajima, Y. Honda, O. Kitao, H. Nakai, T. Vreven, Jr., J. A. Montgomery, J. E. Peralta, F. Ogliaro, M. Bearpark, J. J. Heyd, E. Brothers, K. N. Kudin, V. N. Staroverov, R. Kobayashi, J. Normand, K. Raghavachari, A. Rendell, J. C. Burant, S. S. Iyengar, J. Tomasi, M. Cossi, N. Rega, N. J. Millam, M. Klene, J. E. Knox, J. B. Cross,

V. Bakken, C. Adamo, J. Jaramillo, R. Gomperts, R. E. Stratmann, O. Yazyev, A. J. Austin, R. Cammi, C. Pomelli, J. W. Ochterski, R. L. Martin, K. Morokuma, V. G. Zakrzewski, G. A. Voth, P. Salvador, J. J. Dannenberg, S. Dapprich, A. D. Daniels, Ö. Farkas, J. B. Foresman, J. V. Ortiz, J. Cioslowski and D. J. Fox, *Gaussian 09 Revision A.1*, Gaussian, Inc., Wallingford, CT, 2009.

19 A. D. Becke, *J. Chem. Phys.*, 1993, **98**, 5648.

20 P. J. Stephens, F. J. Devlin, C. F. Chabalowski and M. J. Frisch, *J. Phys. Chem.*, 1994, **98**, 11623.

21 F. Jensen, *Introduction to Computational Chemistry*, John Wiley & Sons Ltd, Chichester, England, 2007.

22 V. Barone and M. Cossi, *J. Phys. Chem. A*, 1998, **102**, 1995.

23 A. Klamt and G. Schuurmann, *J. Chem. Soc., Perkin Trans. 2*, 1993, 799.

24 S. Miertus, E. Scrocco and J. Tomasi, *Chem. Phys.*, 1981, **55**, 117.

25 D. E. Irish and T. Ozeki, in *Analytical Raman Spectroscopy*, ed. J. G. Graselli and B. J. Bulkin, John Wiley & Sons Inc., New York, 1991, p. 60.

26 S. S. Stoyanov, *J. Phys. Chem. A*, 2010, **114**, 5149.

27 I. S. Perelygin, *Opt. Spectrosc.*, 1962, **13**, 198.

28 J. F. Coetzee and W. R. Sharpe, *J. Solution Chem.*, 1972, **1**, 77.

29 I. S. Perelygin and M. A. Klimchuk, *Russ. J. Phys. Chem. (Transl. of Zh. Fiz. Khim.)*, 1973, **47**, 1138.

30 I. S. Perelygin and M. A. Klimchuk, *Russ. J. Phys. Chem. (Transl. of Zh. Fiz. Khim.)*, 1973, **47**, 1402.

31 X. P. Xuan, H. C. Zhang, J. J. Wang and H. Q. Wang, *J. Phys. Chem. A*, 2004, **108**, 7513.

32 J. L. Down, J. Lewis, B. Moore and G. Wilkinson, *J. Chem. Soc.*, 1959, 3767.

33 L. L. Chan and J. Smid, *J. Am. Chem. Soc.*, 1967, **89**, 4547.

34 D. E. Irish and M. H. Brooker, in *Advances in Infrared and Raman Spectroscopy*, ed. R. J. H. Clark and R. E. Hester, Heyden & Son, London, 1977, vol. 2, p. 212.

35 S. Varma and S. B. Rempe, *Biophys. Chem.*, 2006, **124**, 192.

36 P. R. Smirnov and V. N. Trostin, *Russ. J. Gen. Chem.*, 2006, **76**, 175.

37 W. R. Fawcett, G. J. Liu and T. E. Kessler, *J. Phys. Chem.*, 1993, **97**, 9293.

38 D. Brouillette, D. E. Irish, N. J. Taylor, G. Perron, M. Odziemkowski and J. E. Desnoyers, *Phys. Chem. Chem. Phys.*, 2002, **4**, 6063.

39 G. M. Mao, M. L. Saboungi, D. L. Price, M. B. Armand and W. S. Howells, *Phys. Rev. Lett.*, 2000, **84**, 5536.

40 P. Johansson, S. P. Gejji, J. Tegenfeldt and J. Lindgren, *Solid State Ionics*, 1996, **86–88**, 297.

41 P. Johansson, J. Tegenfeldt and J. Lindgren, *Polymer*, 1999, **40**, 4399.

42 O. Borodin, G. D. Smith and R. Douglas, *J. Phys. Chem. B*, 2003, **107**, 6824.

43 A. Maitra and A. Heuer, *Phys. Rev. Lett.*, 2007, **98**, 227802.

44 S. K. Fullerton-Shirey and J. K. Maranas, *Macromolecules*, 2009, **42**, 2142.

45 B. L. Papke, M. A. Ratner and D. F. Shriver, *J. Electrochem. Soc.*, 1982, **129**, 1434.

46 A. Brodin and P. Jacobsson, *Ukr. J. Phys. Opt.*, 2009, **54**, 259.

47 H. F. Matsuura and K. Fukuhara, *J. Polym. Sci., Part A: Polym. Chem.*, 1986, **24**, 383.

48 J. Maxfield and I. W. Shepherd, *Polymer*, 1975, **16**, 505.

49 K. V. Ramana and S. Singh, *Spectrochim. Acta, Part A*, 1988, **44**, 277.

50 R. G. Keil, D. W. Johnson, M. A. Fryling and J. F. Obrien, *Inorg. Chem.*, 1989, **28**, 2764.

51 M. I. S. Sastry and S. Singh, *Curr. Sci.*, 1986, **55**, 1157.

52 F. H. Tukhvatullin, A. Jumabaev, G. Muradov, H. A. Hushvaktov and A. A. Absanov, *J. Raman Spectrosc.*, 2005, **36**, 932.

53 H. Markusson, S. Beranger, P. Johansson, M. Armand and P. Jacobsson, *J. Phys. Chem. A*, 2003, **107**, 10177.

54 A. Eilmes and P. Kubisiak, *J. Phys. Chem. A*, 2010, **114**, 973.